Available online at www.sciencedirect.com
ScienceDirect
Journal of Organometallic Chemistry 693 (2008) 1518–1527
Journal of Organometallic Chemistry
www.elsevier.com/locate/jorganchem

A yellow-emitting iridium complex for use in phosphorescent multiple-emissive-layer white organic light-emitting diodes with high color quality and efficiency ☆

Xiao-Ming Yu [a], Gui-Jiang Zhou [b], Ching-Shan Lam [b], Wai-Yeung Wong [b,*], Xiu-Ling Zhu [a], Jia-Xin Sun [a], Man Wong [a], Hoi-Sing Kwok [a,*]

[a] *Center for Display Research and Department of Electronic and Computing Engineering, The Hong Kong University of Science and Technology, Clear Water Bay, Kowloon, Hong Kong*
[b] *Department of Chemistry and Centre for Advanced Luminescence Materials, Hong Kong Baptist University, Waterloo Road, Hong Kong*

Received 24 September 2007; received in revised form 10 October 2007; accepted 10 October 2007
Available online 22 October 2007

Abstract

A cyclometalated iridium(III) complex containing 2-(9,9-diethylfluoren-2-yl)pyridine [**Ir(Flpy)$_3$**] was prepared and used in the fabrication of both yellow and white organic light-emitting diodes (OLEDs). A hole-blocking material has been used as a hole barrier layer in-between different emission layers, helping the formation of the hole limitation region. With the proper position of a hole barrier layer and the construction of a four-emission-layer structure involving the use of [**Ir(Flpy)$_3$**], the resulting WOLED shows sound device performance as well as very stable color even at high luminances. Such WOLEDs have been demonstrated to reveal superior white light color stability/efficiency trade-off optimization. The Commission Internationale de L'Eclairage (CIE) coordinate differences Δx and Δy are confined to ± 0.015 when the luminance increases from 13 to 14806 cd/m^2. The color rendering index (CRI) of the device is also very good, which varies only from 86 to 87 by changing from the normal direction to 80° off-normal at 12 V. The peak electrophosphorescence efficiency can reach as high as 24.6 cd/A at 168 cd/m^{2}and it can still be kept at 17.2 cd/A at 10834 cd/m^2. Such outstanding performance renders this all-phosphor WOLED very attractive as a white light source for illumination applications, which typically demand high efficiency, high CRI, and stable color in high brightness work conditions.

Keywords: Iridium; Metal complex; Luminescence; Organic light-emitting diode; Phosphorscence

1. Introduction

While the full-color organic light-emitting diodes (OLEDs) have gained tremendous increase in performance over the last decade [1], white OLEDs (WOLEDs) are currently of a growing interest to the lighting research community [2]. Non-pixelated, large area WOLEDs [3] find promising applications as backlights for the liquid crystal display technology and as light sources in the illumination system owing to their potentials for the superior light emission efficiency over traditional incandescent sources in addition to the low-cost and high-throughput manufacturability [4]. However, lighting applications are largely dictated by the need for the WOLED color to be at a particular color point on the blackbody locus as well as the requirement for provision of an adequate color rendering capability for objects viewed in the white light [5].

The precise control of dopants, the demand for an ultra-uniform mixture of colors and the ease of fabrica-

☆ In memory of my mentor, Prof. F. Albert Cotton, for his remarkable contribution to inorganic and organometallic chemistry throughout his life.

* Corresponding authors. Tel.: +852 34117074; fax: +852 34117348 (W.Y. Wong).
E-mail address: rwywong@hkbu.edu.hk (W.-Y. Wong).

0022-328X/$ - see front matter © 2007 Elsevier B.V. All rights reserved.
doi:10.1016/j.jorganchem.2007.10.021

tion steps are all important factors for the WOLEDs to achieve an extremely little color shift with increasing injection current. The fabrication of WOLEDs is relatively more complicated than that of other monochromatic color devices and the color stability is difficult to be maintained at will since an accurate control of at least two dopant concentrations is required. Over the years, a number of device structural concepts have been employed to generate highly efficient white light electrophosphorescence. Among these, one of the most common approaches is to use three separate emitters, each emitting one primary color from red (R), green (G) and blue (B) [6,7]. While the fused organic solid solution method [8] generally requires a careful control over several dopants, it can reduce the fabrication complexity. Tandem (or stacked) WOLEDs consisting of multiple electroluminescent (EL) elements connected in series can also lead to a significant improvement in efficiency [9]. Recently, a novel concept that exploits a blue fluorescent molecule in exchange for a phosphorescent blue dopant furnishes more stable WOLED devices than those mixed with the blue triplet emitters [10]. Keeping a high color stability with a wide driving range and maintaining the EL efficiency at high luminances are still of prominent importance to overcome the hurdle faced nowadays in using WOLEDs as illumination sources and represent one of the major targets in WOLED research for the eventual lighting applications.

In this work, we have synthesized a new yellow (Y) phosphor $[Ir(L)_3]$ (HL = 2-(9,9-diethylfluoren-2-yl)pyridine) [**Ir(Flpy)$_3$**] and demonstrated the exploitation of [**Ir(Flpy)$_3$**] in the fabrication of some WOLEDs with excellent performance in terms of color stability and efficiency. The device consists of a four-emissive-layer architecture (made of B, G, Y and R colors) sandwiched by some charge-injection and -blocking layers without the need for the more sophisticated stacked design [9]. The excitons are effectively confined by the properly interposed hole-blocking material. Saliently, the CIE color coordinate differences can be confined to within ±0.015 when the luminance intensity increases and the CRI value is high and remains almost invariant from the normal to the 80° off-normal direction. The forward emission EL efficiency is as high as 24.6 cd/A at 168 cd/m^{2}and can impressively be kept at ~70% of the peak value (ca. 17.2 cd/A) at a high brightness of 10834 cd/m^2.

2. Results and discussion

2.1. Synthesis, chemical and photophysical characterization of [Ir(Flpy)$_3$]

Scheme 1 shows the synthetic protocol for the homoleptic iridium(III) complex [**Ir(Flpy)$_3$**]. The key compound in our studies is the cyclometalating ligand [**H(Flpy)**], obtained from the Stille coupling of 2-bromo-9,9-diethylfluorene [11] with 2-(tributylstannyl)pyridine in the presence of $[Pd(PPh_3)_4]$. The Ir complex was obtained by direct thermal reaction of $Ir(acac)_3$ with [**H(Flpy)**] in refluxing glycerol [12]. Purification of the mixture by silica chromatography furnished [**Ir(Flpy)$_3$**] as an air-stable orange powder in high purity. It was fully characterized by NMR spectroscopy and FAB-MS spectrometry. The first-order ^{1}H NMR spectrum of [**Ir(Flpy)$_3$**] is consistent with a facial geometry around the Ir center, which indicates that the number of coupled spins is equal to that of protons on one ligand because the three cyclometalating ligands are magnetically equivalent due to the inherent C_3 symmetry of the complex. The parent ion peak at $m/z = 1087$ amu in the FAB mass spectrum confirms its identity.

[**Ir(Flpy)$_3$**] is a highly amorphous and morphologically stable solid and has a high glass transition temperature (T_g) of 118 °C as revealed by differential scanning calorimetry (DSC). It is very thermally stable with onset decomposition temperature determined by thermogravimetric analysis (TGA) to be 441 °C. Also, it can be readily sublimed under vacuum before thermal decomposition was reached.

Photophysical examination of [**Ir(Flpy)$_3$**] reveals that it is characterized by strong absorption bands at $\lambda_{max} = 321$, 336 and 405 nm (Fig. 1). The intense absorptions ($\varepsilon \sim 4.7$–6.0×10^4) at $\lambda_{max} = 321$, 336 nm for [**Ir(Flpy)$_3$**] resemble those for the free ligand [**H(Flpy)**] ($\lambda_{max} = 305$ and 319 nm) and thus can be assigned to the spin-allowed ligand-centered $^1\pi$–π^* transitions. These $^1\pi$–π^* absorption bands below 400 nm are also accompanied by weaker, lower energy features peaking at 405 nm in the visible regime that tail toward 520 nm and they should correspond to an admixture of ^{1}MLCT, ^{3}MLCT and $^3\pi$–π excited states. The strong spin–orbital coupling induced by the heavy-atom effect of Ir center between the singlet and triplet manifolds can give rise to the ^{3}MLCT and $^3\pi$–π bands [13]. [**Ir(Flpy)$_3$**] emits a strong yellow phosphorescence

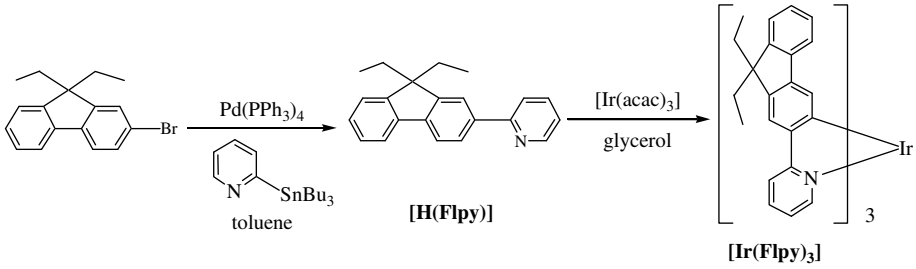

Scheme 1. The synthetic route to the yellow-emitting complex [**Ir(Flpy)$_3$**].

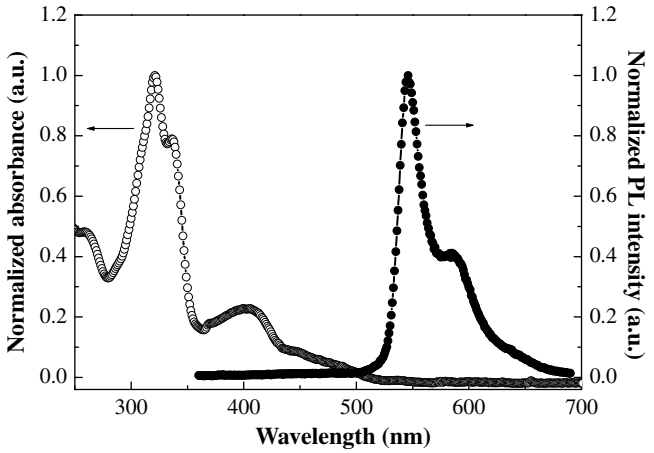

Fig. 1. The UV–Vis and PL spectra for the yellow emitter [**Ir(Flpy)$_3$**] in CH_2Cl_2 at 293 K.

($\lambda_{em} = 545$ nm in CH_2Cl_2, see Fig. 1) from the predominantly ligand-centered $^3\pi$–π^* excited state at the ambient temperature (vs. 360 nm for [**H(Flpy)**]), which are commonplace for other similar iridium cyclometalates [14]. The triplet emission peak displays a large Stokes shift (>100 nm) from the lowest energy absorption peak. The vibronic progression of ca. 1217 cm^{-1} (v_{0-1}) in the emission profile corresponds to the aromatic stretching of the cyclometalated ligands which is characteristic of the substantial involvement of the ligand-centered π–π^* character in the emission. The phosphorescence quantum yield, ϕ_P, recorded in degassed CH_2Cl_2 solution, is 0.49 for [**Ir(Flpy)$_3$**] with a triplet lifetime of ~2.8 μs at 293 K. Accordingly, the radiative lifetime (τ_r) of the triplet excited state deduced from $\tau_r = \tau_P/\phi_P$ is 5.7 μs. The triplet radiative and nonradiative rate constants, k_r and k_{nr}, calculated from σ_P and τ_P using the expressions $\phi_P = \phi_{ISC}\{k_r/(k_r + k_{nr})\}$ and $\tau_P = (k_r + k_{nr})^{-1}$, are both $\sim 1.8 \times 10^5$ s^{-1}, where the intersystem-crossing yield (ϕ_{ISC}) is safely assumed to be 1.0 for metal phosphors with strong heavy-atom effect. No fluorescence signal can be detected at 293 or 77 K.

In the cyclic voltammogram, [**Ir(Flpy)$_3$**] exhibits a reversible anodic wave at 0.22 V, due to the oxidation of the Ir-phenyl center [13]. The reversible reduction occurs primarily on the heterocyclic portion of the cyclometalating ligand at a potential of −2.76 V. Electrochemical data estimated the HOMO and LUMO levels for [**Ir(Flpy)$_3$**] to be −5.02 and −2.04 eV, respectively. These frontier orbital levels are compatible to the energy levels for NPB (HOMO: −5.2 eV) and TPBI (LUMO: −2.9 eV) so that the electronic-structure requirements for the OLEDs can be satisfactorily met (see Table 1).

2.2. Characterization and optimization of yellow-emitting OLEDs

[**Ir(Flpy)$_3$**] is sufficiently stable with respect to sublimation for a fabrication process by the vacuum deposition method. In the first set of experiments, simple yellow light-emitting devices derived from [**Ir(Flpy)$_3$**] were studied and optimized. The structure consists of NPB as the hole transport layer (HTL), CBP doped with [**Ir(Flpy)$_3$**] as the emission layer (EML), TPBI as both the electron transport and hole-blocking layer (ETL/HBL), LiF as the electron injection layer (EIL) and Al as the cathode (Fig. 2). Here, TBPI, instead of the commonly used 2,9-dimethyl-4,7-diphenyl-1,10-phenanthroline (BCP) or tris(8-hydroxyquinolinato)aluminum (Alq_3), was adopted for the devices to effectively confine excitons within the emissive zone since it has a higher electron mobility and hole-blocking ability [15]. To optimize the device efficiency, the thickness of each layer was fixed (HTL 75 nm, EML 20 nm and HBL/ETL 45 nm), while the doping concentration of [**Ir(Flpy)$_3$**] was varied from 2 to 10 wt.%. The EL spectra and their performance characteristics of these yellow-emitting OLEDs are shown in Fig. 3. The EL spectrum resembles its corresponding PL spectrum from thin film, indicating that the same optical transition is responsible for light emission. We chose CBP as the host layer for device fabrication because of the excellent overlap of the UV–Vis absorption of [**Ir(Flpy)$_3$**] with the PL spectrum of CBP, and such guest–host systems meet the requirement for efficient Förster energy transfer from the host singlet to the guest. Emission from the Ir dopant molecules in such devices involves localization of the injected electron and hole on the metal–organic center. It is clear that the major EL peak at 548 nm, with a minor shoulder peak around 588 nm, is independent of the dopant level. The apparent

Table 1
Photophysical, electrochemical and thermal data for **1**

	Absorption[a]	Emission (CH_2Cl_2)		$E_{1/2}^{ox}$ (V)[b]	$E_{1/2}^{red}$ (V)[b]	HOMO (eV)	LUMO (eV)	T_d/T_g (°C)[c]
	λ_{abs} (nm)	λ_{em} (nm) 293 K/77 K[d]	τ_P (μs)[e]					
1	321 (5.99) 336 (4.74) 405 (1.39)	548/545 (0.49)	2.8	0.22	−2.76	−5.02	−2.04	441/118

[a] In degassed CH_2Cl_2 at 293 K and ε (10^4 M^{-1} cm^{-1}) values are shown in parentheses, sh = shoulder.
[b] 0.1 M $[Bu_4N]PF_6$ in THF, vs. Fc/Fc^+ couple.
[c] At a heating rate of 20 °C min^{-1} under N_2.
[d] Φ_P at 293 K is shown in parentheses against *fac*-[Ir(ppy)$_3$] ($\Phi_P = 0.40$), $\lambda_{ex} = 380$ nm.
[e] Triplet lifetime at 293 K.

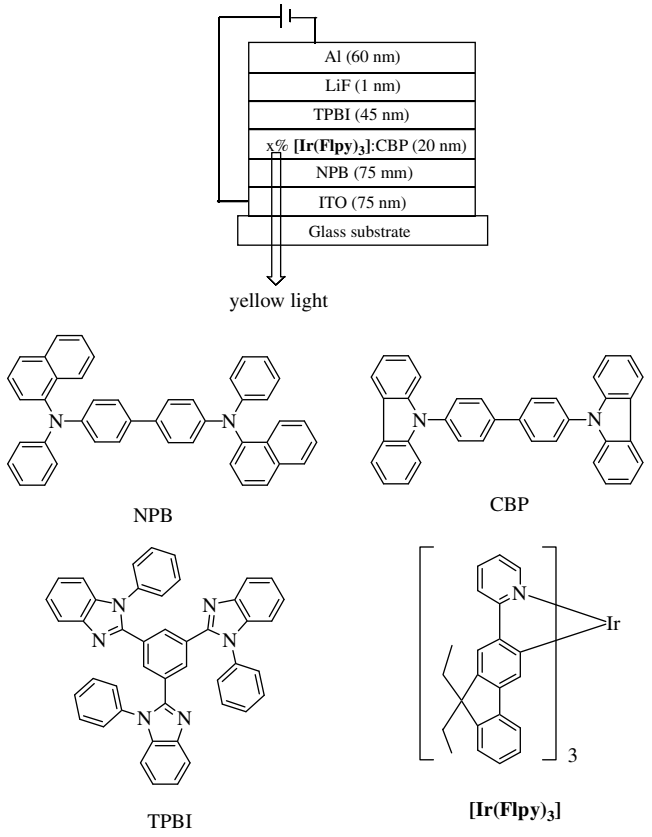

Fig. 2. The general structures for electrophosphorescent OLED devices and the molecular structures of the relevant compounds used in these devices.

yellow emission can be considered to result from mixing green and orange colors in the device. The device with the 2 wt.% doping concentration shows the highest external quantum efficiency (η_{ext}) of 10.3% photons/electron (ph/el), which corresponds to a peak luminance efficiency (η_L) of 36.7 cd/A and a power efficiency (η_P) of 17.7 lm/W (see Table 2 and Supplementary material). The corresponding brightness (L) achieved is $\sim$ 8190 cd/m^2 at 12 V and the CIE color coordinates of such 2% [**Ir(Flpy)$_3$**]-doped OLED are (0.44, 0.55), falling into the yellow region of the chromaticity diagram. Such good device performance suggests the good potential of using [**Ir(Flpy)$_3$**] as a yellow phosphor dye in fabricating high-efficiency WOLEDs.

2.3. Fabrication and characterization of high-performance WOLEDs

2.3.1. Requirements for electrophosphorescent WOLED optimization

For the design of high-quality WOLEDs, the devices should meet not only the emission efficiency requirement but also exhibit some unique features necessary for practical applications. For example, the CIE coordinates of their EL spectra should be located at a particular color point on the blackbody locus for lighting applications in order to provide an adequate color rendering capability for objects viewed in the white light. To fulfill these concerns, several strategies have been employed in the present work and WOLEDs with novel structures have been devised that can show high efficiency, desirable CIE coordinates and high CRI.

2.3.2. Thickness optimization for hole barrier layer between two emission layers

From previous experience and literature reports, it is required to deposit the orange emission layer first, followed by the blue emission layer in the initial WOLED fabrication in order to achieve a better white CIE balance [16]. Experimentally, we try to obtain stable white light EL spectrum with reasonable CIE coordinates by inserting a thin hole barrier layer of TPBI (abbreviated as TL) between the red-emitting layer (RL) and blue-emitting layer (BL) to balance the distribution of the holes in RL and BL. The device structure of ITO (75 nm)/NPB (40 nm)/RL (15 nm)/TL (x nm)/BL (15 nm)/TPBI (25 nm)/LiF (1 nm)/Al (120 nm) was fabricated in which the RL consists of 10% bis(2-benzo[b]thiophen-2-ylpyridine)(acetylacetonate)iridium(III), [(btp)$_2$Ir(acac)], doped in CBP whereas the BL is made of 8% iridium(III) bis[(4,6-difluorophenyl)pyridinato-N,C^2]picolinate, [FIrPic], doped in N,N'-dicarbazolyl-3,5-benzene (mCP). These two-element

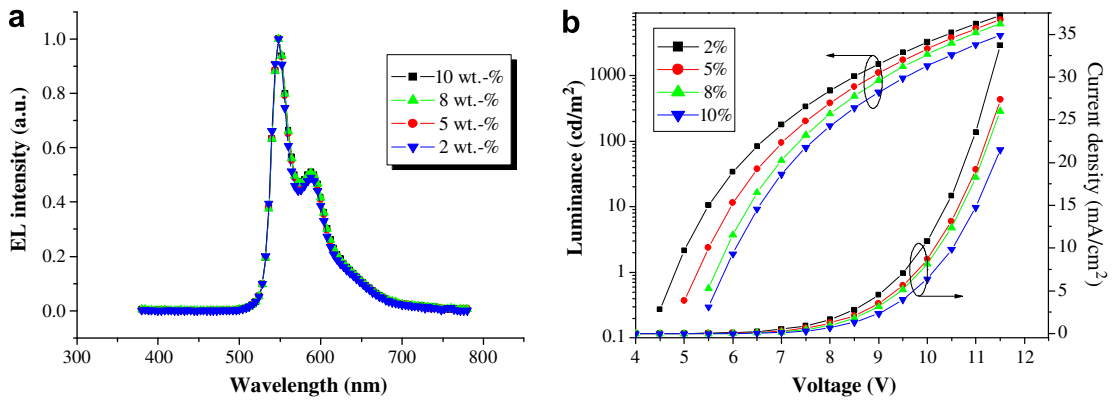

Fig. 3. (a) EL spectra and (b) luminance–voltage–current density curves of the yellow-emitting OLEDs doped with [**Ir(Flpy)$_3$**] at 10 V.

Table 2
Performance of electrophosphorescent yellow OLEDs

Phosphor dopant	$V_{turn\text{-}on}$ (V)	Max. luminance L_{max} (cd/m^2)[a]	η_{ext} (%)	η_L (cd/A)	η_p (lm/W)	λ_{max} (nm)[b]
2 wt.%	5.0	8189 (12)	9.9[c]	35.1	16.8	548 (0.44, 0.55)
			9.8[d]	34.6	12.7	
			10.3 (7.5)[a]	36.7 (7.5)	17.7 (6.0)	
5 wt.%	5.4	7047 (12)	8.4[c]	29.5	13.2	548 (0.45, 0.55)
			8.9[d]	31.3	11.1	
			9.0 (8.5)[a]	31.8 (8.5)	14.9 (6.0)	
8 wt.%	5.6	6128 (12)	7.3[c]	25.8	11.0	548 (0.45, 0.54)
			7.6[d]	26.7	9.2	
			7.7 (8.0)[a]	27.1 (8.0)	11.4 (7.0)	
10 wt.%	5.7	4111 (12)	7.2[c]	25.1	10.4	548 (0.45, 0.54)
			6.5[d]	22.7	7.5	
			7.4 (7.0)[a]	26.1 (7.0)	11.7 (7.0)	

[a] Maximum luminance of the devices. Values in parentheses are the voltages at which they were obtained.
[b] CIE coordinates $[x, y]$ in parentheses.
[c] Values collected at 100 cd/m^2.
[d] Values collected at 1000 cd/m^2.

WOLEDs were also optimized with different thickness of TL. From the EL spectra at 8 V shown in Fig. 4, we note that each of them exhibits two close peaks at 472 and 496 nm, which arise from the blue phosphor FIrPic, and a sharp peak at 560 nm (with a shoulder at ~671 nm) due to the red electrophosphorescence from [$(btp)_2$Ir(a-cac)]. Based on these studies at different driving voltages (see Fig. 4 and Supplementary material), we can see that for the device without TL, nearly all the holes rush into the BL and combine with electrons to give the intense blue band in its EL spectra with only a very weak red light component. With a thick TL layer (4 nm), it will confine too much holes in the RL at low driving voltage because of the hole-blocking property of TPBI, which results in a greater variation of the EL spectra with the driving voltage. We found that more stable EL spectra were obtained with 2 nm TL compared to those with 4 nm TL, so the thickness of TL was set to 2 nm for the hole barrier layer in the following WOLED optimization.

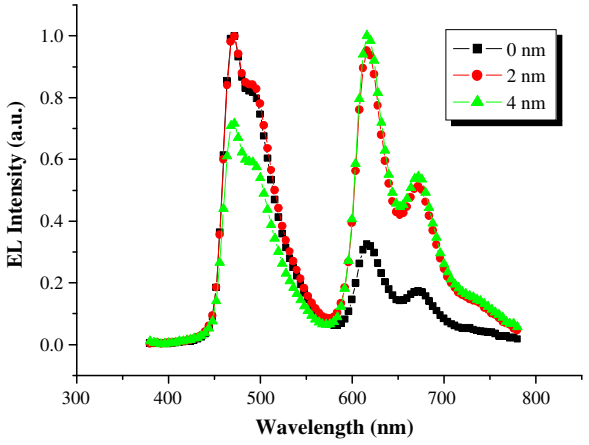

Fig. 4. EL spectra for two-element WOLEDs with different thickness of the hole barrier layer at 8 V.

2.3.3. Position optimization for the hole barrier layer

For the sake of improving the performance of WOLEDs with multiple-emissive-layer, a sandwiched structure with a long-wavelength emission layer between two shorter-wavelength emission layers is usually adopted [17]. In such structure, the red dopant absorbs the energy from the blue dopant in the first BL and the emission from the second BL will compensate for the energy loss of the blue light in the resulting EL spectrum especially at low driving voltage. Hence, the internal EL efficiency would be enhanced. In view of this concept and the results discussed above for the functional role of TL, the devices with the emissive-layer structures [BL (15 nm)/RL (15 nm)/BL (6 nm)] (BRB), [BL (15 nm)/TL (2 nm)/RL (15 nm)/BL (6 nm)] (BTRB) and [BL (15 nm)/RL (15 nm)/TL (2 nm)/BL (6 nm)] (BRTB) were fabricated to test the necessity of the hole barrier layer and its proper position in the device. The EL spectra at different driving voltages for the three devices are shown in Fig. 5.

The CIE coordinate difference, $(\Delta x, \Delta y)$, is $(0.06, 0.01)$ for BRB, $(0.03, 0.01)$ for BTRB and $(0.03, 0.01)$ for BRTB devices, respectively, as the voltage increases from 8 to 16 V. Evidently, we can see that the BTRB device with TL between the first BL and RL shows more balanced EL spectra for white light (Fig. 5b) among the three cases, i.e. with a higher white color stability. But, there is still room for an even better white color chromaticity which could be achieved by adjusting other factors in the multiple-emission-layer.

2.3.4. Compensation of the green component in the EL spectra of WOLEDs

Many reported WOLEDs with dual emission layers typically display an obvious valley in the green light region of their EL spectra [18]. Although such drawback can be partially tackled with the tail emission from the BL, the EL spectra still lack a proper green light for practical application. So, a green-emitting layer (GL) consisting of 8% tris(2-phenylpyridine)iridium(III), [$Ir(ppy)_3$], doped in CBP was inserted to the WOLEDs. After optimization of the sequence of the emission layers and the layer thickness, the proper structure for the emission layer was fixed as [BL (10 nm)/TL (2 nm)/RL (5 nm)/GL (20 nm)] (BTRG).

Fig. 6 shows the EL spectra of the device at different driving voltages from 8 to 16 V. From the spectral pattern, we see that the green light component is enhanced greatly and the EL spectra are stable with variation of Δx and Δy both in the range of ± 0.02. The result shows that introducing GL can effectively compensate for the green light deficiency in the EL spectra of WOLEDs by a careful

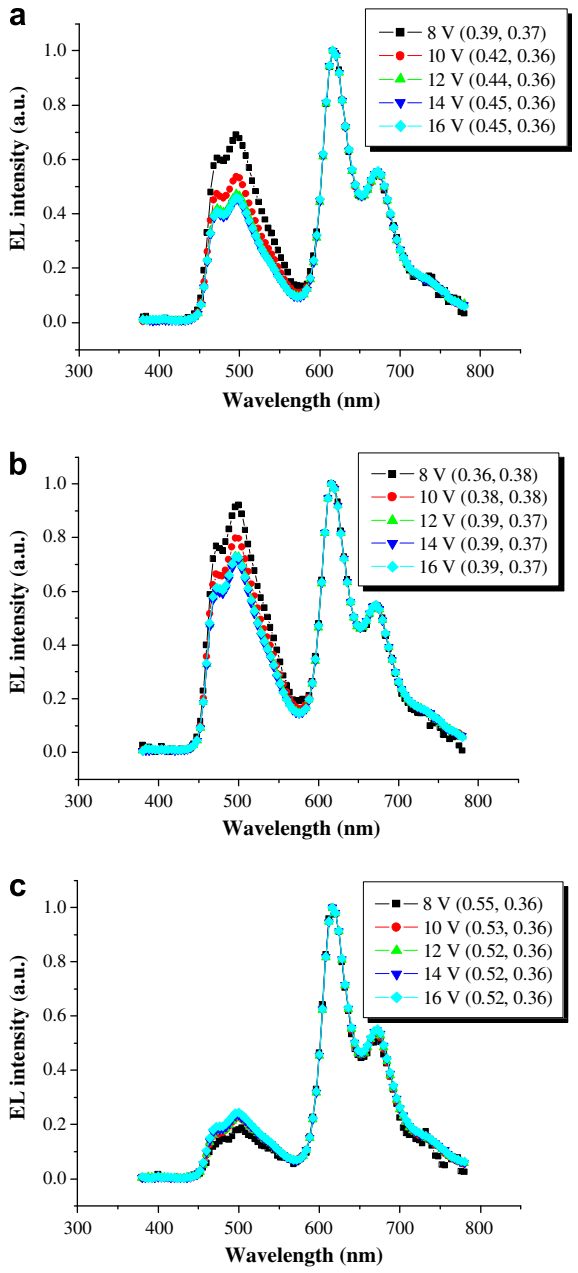

Fig. 5. EL spectra of OLEDs with the emissive-layer structures: (a) BRB, (b) BTRB and (c) BRTB and the CIE data at different voltages are shown in the inset in each case.

design of the emission-layer structure. However, the over-dosed green light component together with the presence of a valley in the yellow light region indicate that further optimization for the emission structure of WOLEDs is still desired in order to obtain an ideal white light chromaticity.

2.3.5. High-performance WOLEDs with four-color emission layer

In order to balance the light components at all wavelengths in the EL spectra of WOLEDs, a yellow emission layer (YL) containing [**Ir(Flpy)$_3$**] ($\lambda_{max} = 546$ nm) was finally inserted based on the results aforesaid. From Section 2.2, the maximum current efficiency can surpass

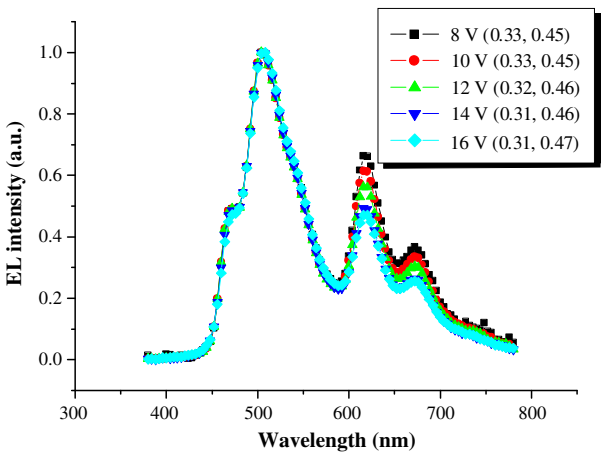

Fig. 6. EL spectra of devices with the emissive-layer structure of BTRG.

30 cd/A with the EL peak at 560 nm, which is an ideal wavelength for the yellow light. So a YL with 4% [**Ir(Flpy)$_3$**] in CBP was combined with BL, RL, GL and TL to form the four-color emitting layer for WOLEDs. The proper position for TL was also assessed. Two different combinations were adopted for EML, namely, [BL (10 nm)/TL (2 nm)/RL (7 nm)/YL (8 nm)/GL (10 nm)] (BTRYG) and [BL (10 nm)/RL (7 nm)/TL (2 nm)/YL (8 nm)/GL (10 nm)] (BRTYG). The EL spectra (Fig. 7) and CIE coordinates (Table 3 and Fig. 8) indicate that such four-color emitting system with the proper insertion of TL is a very effective way to achieve a stable white light with ideal color chromaticity, and a well-balanced spectrum among components of all different colors.

CIE coordinates, CRI and correlated color temperature (CCT) are the three critical parameters defining the color quality of a white light source. The CCT of our white device was calculated from the CIE coordinates using the formula reported by McCamy [19] and the CRI calculated from the EL spectrum of the device by the CIE CRI method [20]. At 12 V, the device with BTRYG structure exhibits a CRI of 81 and a CCT of 6122 K. The corresponding values are 86 and 3864 K, respectively for device with BRTYG structure. CRI, which is a parameter to define how true the color of an object appears when illuminated under it, is measured in the 0–100 scale, with 100 being the highest ability for color rendering. The CRI values are typically 80, 90 and 75 for the incandescent source, fluorescent light and the reported white OLEDs, respectively [21]. The majority of WOLEDs shows CRI of 75–80 or below, which are lower than that of fluorescent light sources and not good enough for a lighting source [6a,22]. Recently, Niu et al. have developed white devices with high CRI value of up to 92 by doping a white-emitting polymer (consisting of blue and orange fluorescent moieties) with a red phosphorescent dopant to broaden its emission spectrum [23]. Encouragingly, our current approach gives highly efficient WOLEDs with CRI as high as 86 which will provide a guidance toward the improvement of the CRI of WOLEDs. Moreover, it is clear that the BRTYG device is

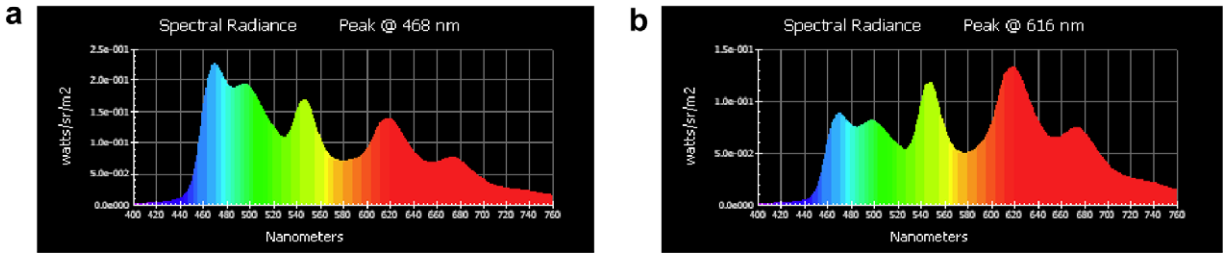

Fig. 7. EL spectra of WOLEDs with four-emissive-layer structures: (a) BTRYG and (b) BRTYG.

Table 3
The CIE coordinates of the WOLED devices with multiple-emissive-layer structures: (a) [BL (10 nm)/TL (2 nm)/RL (7 nm)/YL (8 nm)/GL (10 nm)] and (b) [BL (10 nm)/RL (7 nm)/TL (2 nm)/YL (8 nm)/GL (10 nm)]

Driving voltage (V)	(a) BTRYG	(b) BRTYG
6	0.30, 0.39	0.38, 0.42
8	0.32, 0.37	0.40, 0.39
10	0.32, 0.38	0.40, 0.40
12	0.31, 0.38	0.39, 0.41
14	Not measured	0.37, 0.41

more warm and more suitable to meet illumination specifications [2a].

It is worth noting that both Δx and Δy are well controlled to within the narrow range of ± 0.015 in these two four-emissive-layer devices, in which Δx undergoes a slight rise and down, while Δy experiences the opposite trend. Such a small shift is a good manifestation of the proper use and interposition of the hole barrier layer which efficiently confines the excitons in-between the four-emission-layer. In fact, the mobility of hole is about 100 times higher than that of electrons inside the organic material. In a single-emission-layer device, the excitons are usually formed in the emission layer near the cathode at low driving voltages but will be shifted to a region near anode. When the hole barrier layer is inserted after the first or the second emission layer (as viewed from the anode side) in the multiple-emissive-layer devices, holes are confined efficiently to a particular area especially under a low driving voltage. At the same time, electrons could not travel far enough due to the low internal electrical field. The distribution profiles of the holes and electrons are similar but follow opposite directions. When the driving voltage increases, more holes can jump through the barrier layer and more electrons can travel further, again resulting in similar distribution profiles of holes and electrons. In these two cases, the excitons (as decided by the electron–hole pairs) in the emission layer will increase with the driving voltage but their distribution is almost identical inside the whole emission area. So, the CIE coordinates could maintain more or less constant during the whole driving process

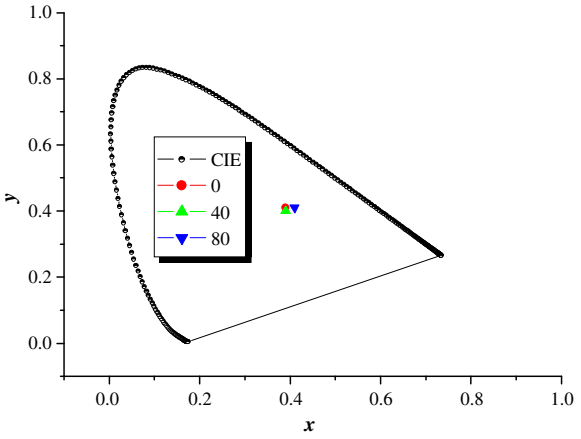

Fig. 9. Variation of the CIE coordinates with the viewing direction: normal to the emission face (●), 40° from normal direction (▲), and 80° from normal direction (▼).

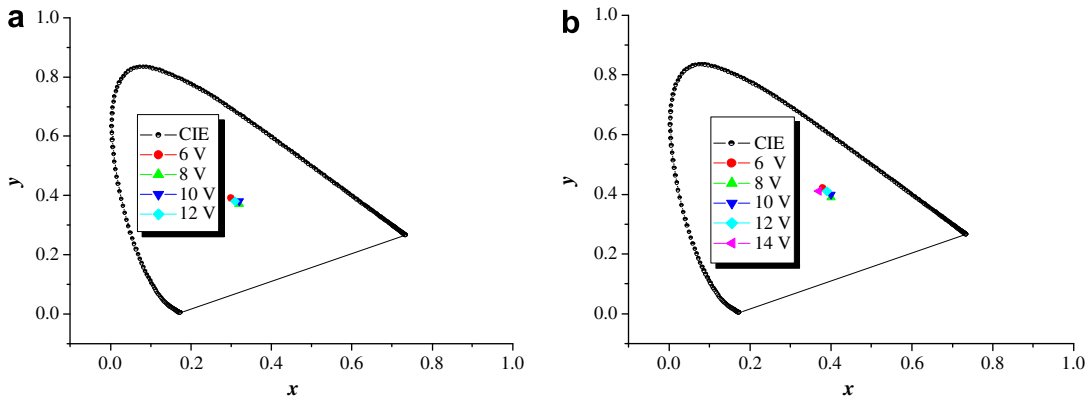

Fig. 8. Variation of the CIE coordinates of WOLEDs with voltages for the emitting layer structures: (a) BTRYG and (b) BRTYG.

and such desirable color stability should be advantageous for lighting applications.

2.3.6. Light emission performance with outcoupling lens

The WOLED performance can be improved by enhancing the outcoupling efficiency (η_{OC}). To achieve this, the luminaire was optically coupled to the OLED glass substrate (see Supplementary material). Luminaire increases the amount of outcoupled light by reducing wave guiding in the glass substrate and hence η_{OC} can be enhanced [24]. One outcoupling lens was fabricated near the emission side of the device. Additionally, it is interesting that the color changes very little from different viewing angles at 12 V (Fig. 9). The CRI is 86 in the normal direction, and is only shifted to 87 as observed at 80° from the normal direction.

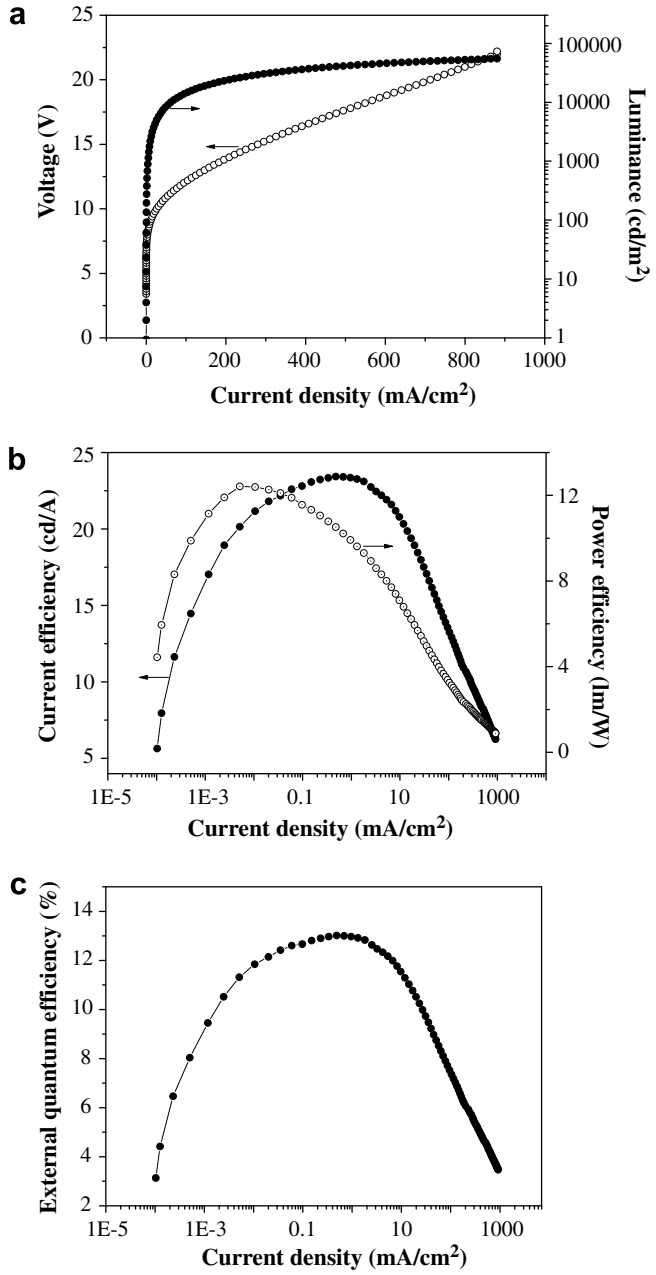

Fig. 10. (a) Voltage–current density–luminance and (b) current and power efficiency vs. current density and (c) EQE vs. current density characteristics of the device with BRTYG structure.

Fig. 10 shows the driving voltage–current density–luminance and EL efficiency–current density characteristics of the device with BRTYG structure. The device can achieve maximum $\eta_{ext} = 13.0\%$ (at 0.48 mA/cm^2 and 136 cd/m^2) and the peak η_L and η_P are 23.4 cd/A and 12.4 lm/W, respectively. The efficiency can still maintain 54% of the highest η_{ext} when the luminance is raised to 19977 cd/m^2. Our device performs better than some of the best two-element all-fluorescent WOLEDs with sky-blue dopants (11–17 cd/A) [16a], and all-phosphor-doped devices (17 cd/A) recently reported [16b], together with an improved white light efficiency/color purity trade-off. As a small device approximation, the maximum total power efficiency (η_t) of our WOLED is 21.1 lm/W (c.f. $\eta_t = 12$–17 lm/W for a typical incandescent light bulb) [2a].

3. Conclusions

By employing a hole barrier layer to control the distribution of excitons in the emitting layer, the color stability can be effectively enhanced in the multiple-emissive-layer WOLEDs based on a yellow-emitting iridium phosphor. Highly efficient WOLEDs based on four-color multiple-emissive-layer coupled with the appropriate usage of the outcoupling setting were achieved that can exhibit high color stability with respect to an increase in the driving condition and viewing angle. After optimization of the WOLED device structure for the electrical and optical performance, the highest efficiencies reach 23 cd/A and 13% ph/el, corresponding to a maximum total power efficiency of ~21 lm/W. Given the device performance advantage (in terms of light emission efficiency, color purity and color stability), the present study will act as an inspiration to address the WOLED efficiency/color purity trade-off issue which is still a key problem for high-performance design. Such work will certainly impact positively on the future advance of both passive and active matrix full-color OLEDs.

4. Experimental

4.1. Equipment and physical measurements

NMR spectra were measured in $CDCl_3$ on a JEOL EX270 or a Varian Inova 400 MHz FT-NMR spectrometer, with the chemical shifts quoted relative to Me_4Si. Electron impact (EI) and fast atom bombardment (FAB) mass spectra were recorded on a Finnigan MAT SSQ710 system. UV–Vis spectra were obtained on the HP-8453 spectrophotometer. The photoluminescent properties and lifetime were investigated on the Photon Technology International (PTI) Fluorescence Master Series QM1 system. The phosphorescence quantum yield of [**Ir(Flpy)$_3$**] was determined in CH_2Cl_2 solution at 293 K against *fac*-[Ir(ppy)$_3$]

(Hppy = 2-phenylpyridine) as a reference ($\Phi_P = 0.40$) [25]. Electrochemical measurements were made in THF using a Princeton Applied Research (PAR) model 273 A potentiostat. A conventional three-electrode configuration consisting of a glassy carbon working electrode, and Pt-wires as both the counter and reference electrodes was used. The supporting electrolyte was 0.1 M $[Bu_4N]PF_6$. Ferrocene was added as an internal standard after each set of measurements, and all potentials reported were quoted with reference to the ferrocene-ferrocenium (Fc/Fc^+) couple at a scan rate of 100 mV/s. The oxidation (E_{ox}) and reduction (E_{red}) potentials were used to determine the HOMO and LUMO energy levels using the equations $E_{HOMO} = -(E_{ox} + 4.8)$ eV and $E_{LUMO} = -(E_{red} + 4.8)$ eV which were calculated using the internal standard ferrocene value of −4.8 eV with respect to the vacuum [26]. Thermal analyses were performed with the Perkin-Elmer Pyris Diamond DSC and Perkin-Elmer TGA6 thermal analyzers at a heating rate of 20°/min.

4.2. General information for synthesis

All the commercially available reagents and chemicals were purchased from Aldrich or Acros. They were used directly without further purification unless otherwise stated. Solvents were carefully dried and distilled from appropriate drying agents prior to use (sodium benzophenone-ketyl for hexane, THF and toluene, CaH_2 for CH_2Cl_2). All reactions were performed under nitrogen and monitored by thin-layer chromatography (TLC) with Merck pre-coated glass plates. Compounds were visualized with UV light irradiation at 254 and 365 nm. Flash column chromatography and preparative TLC were carried out using silica gel from Merck (230–400 mesh) at room temperature (rt).

4.3. Syntheses of 2-(9,9-diethylfluoren-2-yl)pyridine [H(Flpy)]

2-Bromo-9,9-diethylfluorene [11] (0.45 g, 1.50 mmol) and 2-(tributylstannyl)pyridine (0.61 g, 1.66 mmol) were mixed in dry toluene (30 mL) and $Pd(PPh_3)_4$ (0.18 g, 0.15 mmol) was then added to the solution to carry out the Stille-type coupling [27]. The resulting mixture was stirred at 110 °C for 24 h. After cooling to rt, the reaction mixture was poured into a separating funnel and CH_2Cl_2 (100 mL) was added followed by washing with water (3 × 50 mL). The organic phase was dried over $MgSO_4$. Then the solvent was removed and the crude product was purified by column chromatography eluting with CH_2Cl_2/hexane (3:1, v/v). The title product was obtained as a white solid (0.34 g, 75%). ^1H NMR ($CDCl_3$): δ 8.71 (dd, $J = 0.8$, 4.9 Hz, 1 H, Ar), 8.06 (d, $J = 1.6$ Hz, 1H, Ar), 7.59 (dd, $J = 1.6$, 7.8 Hz, 1H, Ar), 7.78–7.61 (m, 4H, Ar), 7.33–7.29 (m, 3H, Ar), 7.15–7.10 (m, 1H, Ar), 2.17–1.99 (m, 4H, Et), 0.35 (t, $J = 7.3$ Hz, 6H, Et). $^{13}C\{^1H\}$ NMR ($CDCl_3$): δ 157.38, 150.20, 150.10, 149.30, 142.23, 140.71, 137.93, 136.36, 127.10, 126.63, 125.62, 122.66, 121.58, 121.02, 120.29, 119.71, 119.59 (Ar), 56.15 (quat. C), 32.68, 8.55 (Et). FAB-MS (m/z): 299 [M^+]. Anal. Calc. for $C_{22}H_{21}N$: C, 88.25; H, 7.07; N, 4.68. Found: C, 88.10; H, 6.99; N, 4.78%. λ_{max} ($\varepsilon \times 10^{-4}/M^{-1}\,cm^{-1}$): 305 (4.23), 319 (4.31) nm. PL (CH_2Cl_2): λ_{em} 360 nm.

4.4. Synthesis of [Ir(Flpy)$_3$]

[**Ir(acac)$_3$**] (0.15 g, 0.30 mmol) and [**H(Flpy)**] (0.32 g, 1.07 mmol) were mixed in glycerol (16 mL) under a N_2 atmosphere. While the reaction mixture was allowed to react at 220 °C overnight, it was cooled to rt and water (60 mL) was then added. The resulting mixture was extracted with CH_2Cl_2 (3 × 100 mL) and the organic phase was dried over $MgSO_4$. Upon the removal of solvent under vacuum, the residue was purified by column chromatography using CH_2Cl_2 as the eluent to afford the title compound as an orange solid (0.08 g, 25%). ^1H NMR ($CDCl_3$): δ 7.96 (d, $J = 8.1$ Hz, 3 H, Ar), 7.68–7.54 (m, 9H, Ar), 7.22–7.10 (m, 12H, Ar), 6.99–6.96 (m, 3H, Ar), 6.86–6.84 (m, 3H, Ar), 2.03 (m, 12H, Et), 0.49–0.31 (m, 18H, Et). FAB-MS (m/z): 1087 [M^+]. Anal. Calc. for $C_{66}H_{60}N_3Ir$: C, 72.90; H, 5.56; N, 3.86. Found: C, 72.82; H, 5.45; N, 3.98%.

4.5. OLED fabrication and measurements

Commercial indium tin oxide (ITO) coated glass with sheet resistance of 25 Ω/square was used as the starting substrates. Before device fabrication, the cleaned ITO glass substrates were modified by tetrafluoride carbon plasma (DC 180 V, 20 Pa) for 20 s followed by ozone treatment for 10 min. The OLED devices were fabricated in a high vacuum evaporation system at a base pressure less than 2×10^{-4} Pa without breaking vacuum between each vacuum deposition process. Each device was generally assembled in the sequence: ITO on glass substrate (anode), 40 nm of 4,4′-bis[*N*-(1-naphthyl)-*N*-phenylamino]biphenyl (NPB), single or multiple-emissive layer, 25 nm of 2,2′,2″-(1,3,5-phenylene)tris(1-phenyl-1H-benzimidazole) (TPBI), 1 nm of LiF and 120 nm of Al (cathode). The emissive layer was formed by co-deposition of the dopant and the triplet host. The layer thickness during evaporation was monitored in situ using a quartz crystal oscillator. The active area of the device was 5 mm^2 as defined by the shadow mask. The electrical and optical characteristics of these devices were measured using R6145 DC voltage current source, FLUKE 45 dual display multimeter and Spectrascan PR650 spectrophotometer in a dark room under ambient air condition.

Acknowledgements

W.-Y.W. thanks the Hong Kong Research Grants Council (Grant No.: HKBU 2021/06P) and the Hong

Kong Baptist University for the financial support of this work.

Appendix A. Supplementary material

Supplementary data associated with this article can be found, in the online version, at doi:10.1016/j.jorganchem.2007.10.021.

References

[1] (a) Z. Shen, P.E. Burrows, V. Bulović, S.R. Forrest, M.E. Thompson, Science 276 (1997) 5321;
(b) P.E. Burrows, G. Gu, V. Bulović, Z. Shen, S.R. Forrest, M.E. Thompson, IEEE Trans Electron. Dev. 44 (1997) 1188;
(c) M.A. Baldo, M.E. Thompson, S.R. Forrest, Nature 403 (2000) 750.
[2] (a) A. Misra, P. Kumar, M.N. Kamalasanan, S. Chandra, Semicond. Sci. Technol. 21 (2006) R35;
(b) B.W. D'Andrade, S.R. Forrest, Adv. Mater. 16 (2004) 1585;
(c) A.J. Heeger, Solid State Commun. 107 (1998) 673;
(d) H. Kanno, Y. Sun, S.R. Forrest, Appl. Phy. Lett. 86 (2005) 263502;
(e) T. Fuhrmann, J. Salbeck, MRS Bull. 28 (2003) 354.
[3] A.R. Duggal, J.J. Shiang, D.F. Foust, L.G. Turner, W.F. Nealon, J.C. Bortscheller, SID Digest (2005) 28.
[4] R.F. Service, Science 310 (2005) 1762.
[5] (a) Optoelectronics Industry Development Association (OIDA) Department of Energy – Office of Building Technology, State and Community Programs, OLEDs Update, 2002;
(b) B.W. D'Andrade, S.R. Forrest, Adv. Mater. 16 (2004) 1585.
[6] (a) B.W. D'Andrade, R.J. Holmes, S.R. Forrest, Adv. Mater. 16 (2004) 624;
(b) R.J. Holmes, B.W. D'Andrade, X. Ren, J. Li, M.E. Thompson, S.R. Forrest, Appl. Phys. Lett. 83 (2003) 3818.
[7] (a) J. Kido, M. Kimura, K. Nagai, Science 267 (1995) 1332;
(b) B.W. D'Andrade, M.E. Thompson, S.R. Forrest, Adv. Mater. 14 (2002) 147;
(c) G. Cheng, Y. Zhang, Y. Zhao, Y. Lin, C. Ruan, S. Liu, T. Fei, Y. Ma, Y. Cheng, Appl. Phys. Lett. 89 (2006) 043504;
(d) Y. Shao, Y. Yang, Appl. Phys. Lett. 86 (2005) 073510.
[8] (a) G. Lei, L. Wang, Y. Qiu, Appl. Phys. Lett. 85 (2005) 5403;
(b) Y. Shao, Y. Yang, Appl. Phys. Lett. 86 (2005) 073510.
[9] (a) H. Kanno, R.J. Holmes, Y. Sun, S. Kena-Cohen, S.R. Forrest, Adv. Mater. 18 (2006) 339;
(b) C. Chang, J. Chen, S. Hwang, C.H. Chen, Appl. Phys. Lett. 87 (2005) 253501.
[10] (a) Y. Sun, N.C. Giebink, H. Kanno, B. Ma, M.E. Thompson, S.R. Forrest, Nature 440 (2006) 908;
(b) G. Schwartz, K. Fehse, M. Pfeiffer, K. Walzer, K. Leo, Appl. Phys. Lett. 89 (2006) 083509.
[11] (a) M.S. Khan, M.R.A. Al-Mandhary, M.K. Al-Suti, B. Ahrens, M.F. Mahon, L. Male, P.R. Raithby, C.E. Boothby, A. Köhler, Dalton Trans. (2003) 74;
(b) L. Liu, W.-Y. Wong, Y.-W. Lam, W.-Y. Tam, Inorg. Chim. Acta 360 (2007) 109.
[12] (a) K. Dedeian, P.I. Djurovich, F.O. Garces, G. Carlson, R.J. Watts, Inorg. Chem. 30 (1991) 1685;
(b) A.B. Tamayo, B.D. Alleyne, P.I. Djurovich, S. Lamansky, I. Tsyba, N.N. Ho, R. Bau, M.E. Thompson, J. Am. Chem. Soc. 125 (2003) 7377;
(c) S. Lamansky, P. Djurovich, D. Murphy, F. Abdel-Razzaq, H.-E. Lee, C. Adachi, P.E. Burrows, S.R. Forrest, M.E. Thompson, J. Am. Chem. Soc. 123 (2001) 4304;
(d) S. Okada, K. Okinaka, H. Iwawaki, M. Furugori, M. Hashimoto, T. Mukaide, J. Kamatani, S. Igawa, A. Tsuboyama, T. Takiguchi, K. Ueno, Dalton Trans. (2005) 583;
(e) S. Jung, Y. Kang, H.-S. Kim, Y.-H. Kim, C.-L. Lee, J.-J. Kim, S.-K. Lee, S.-K. Kwon, Eur. J. Inorg. Chem. (2004) 3415.
[13] (a) J.C. Ostrowski, M.R. Robinson, A.J. Heeger, G.C. Bazan, Chem. Commun. (2002) 784;
(b) S. Bettington, M. Tavasli, M.R. Bryce, A. Beeby, H. Al-Attar, A.P. Monkman, Chem. Eur. J. 13 (2007) 1423;
(c) M. Tavasli, S. Bettington, M.R. Bryce, H.A. Al Attar, F.B. Dias, S. King, A.P. Monkman, J. Mater. Chem. 15 (2005) 4963;
(d) W.-Y. Wong, G.-J. Zhou, X.-M. Yu, H.-S. Kwok, B.-Z. Tang, Adv. Funct. Mater. 16 (2006) 838.
[14] (a) P.-T. Chou, Y. Chi, Chem. Eur. J. 13 (2007) 380;
(b) H. Yersin, Top. Curr. Chem. 241 (2004) 1;
(c) M.W. Langeveld, U.S. Schubert, Adv. Mater. 17 (2005) 1109;
(d) M.A. Baldo, M.E. Thompson, S.R. Forrest, Pure Appl. Chem. 71 (1999) 2095;
(e) R.C. Evans, P. Douglas, C.J. Winscom, Coord. Chem. Rev. 250 (2006) 2093;
(f) P.L. Burn, S.-C. Lo, I.D.W. Samuel, Adv. Mater. 19 (2007) 1675.
[15] (a) K.M.-C. Wong, X. Zhu, L.-L. Hung, N. Zhu, V.W.-W. Yam, H.-S. Kwok, Chem. Commun. (2005) 2906;
(b) J.-P. Duan, P.-P. Sun, C.-H. Cheng, Adv. Mater. 15 (2003) 224;
(c) C.H. Chen, J. Shi, C.W. Tang, Macromol. Symp. 125 (1997) 1.
[16] (a) M.-F. Lin, L. Wang, W.-K. Wong, K.-W. Cheah, H.-L. Tam, M.-T. Lee, M.-H. Ho, C.H. Chen, Appl. Phys. Lett. 91 (2007) 1;
(b) X.-M. Yu, H.-S. Kwok, W.-Y. Wong, G.-J. Zhou, Chem. Mater. 18 (2006) 5097.
[17] G. Cheng, Y. Zhang, Y. Zhao, Y. Lin, C. Ruan, S. Liu, T. Fei, Y. Ma, Y. Cheng, Appl. Phys. Lett. 89 (2006) 043504.
[18] (a) J. Liu, Q. Zhou, Y. Cheng, Y. Geng, L. Wang, D. Ma, X. Jing, F. Wang, Adv. Funct. Mater. 16 (2006) 957;
(b) G.L. Tu, Q.G. Zhou, Y.X. Cheng, L.X. Wang, D.G. Ma, X.B. Jing, F.S. Wang, Appl. Phys. Lett. 85 (2004) 2172;
(c) G.L. Tu, C.Y. Mei, Q.G. Zhou, Y.X. Cheng, Y.H. Geng, L.X. Wang, D.G. Ma, X.B. Jing, F.S. Wang, Adv. Funct. Mater. 16 (2006) 101;
(d) W.F. Xie, S.L. Chew, C.S. Lee, S.T. Lee, P.F. Wang, H.L. Kwong, J. Appl. Phys. 100 (2006) 096114.
[19] C.S. McCamy, Color Res. Appl. 17 (1992) 142.
[20] Method of Measuring and Specifying Color Rendering Properties of Light Sources, CIE, Paris, 1974.
[21] (a) Z.S. Su, G.B. Che, W.L. Li, W.M. Su, M.T. Li, B. Chu, B. Li, Appl. Phys. Lett. 88 (2006) 213508;
(b) B.W. D'Andrade, J. Brooks, V. Adamovich, M.E. Thompson, S.R. Forrest, Adv. Mater. 14 (2002) 1032.
[22] (a) G. Cheng, Y.F. Zhang, Y. Zhao, S.Y. Liu, Appl. Phys. Lett. 88 (2006) 083512;
(b) B.W. D'Andrade, S.R. Forrest, J. Appl. Phys. 94 (2003) 3101.
[23] X. Niu, L. Ma, B. Yao, J. Ding, G. Tu, Z. Xie, L. Wang, Appl. Phys. Lett. 89 (2006) 213508.
[24] B.W. D'Andrade, J.J. Brown, Appl. Phys. Lett. 88 (2006) 192908.
[25] K.A. King, P.J. Spellane, R.-J. Watts, J. Am. Chem. Soc. 107 (1985) 1431.
[26] (a) M. Thelakkat, H.-W. Schmidt, Adv. Mater. 10 (1998) 219;
(b) R.S. Ashraf, M. Shahid, E. Klemm, M. Al-Ibrahim, S. Sensfuss, Macromol. Rapid Commun. 27 (2006) 1454.
[27] J.K. Stille, Angew. Chem. Int. Ed. 25 (1986) 508.